

On the critical signatures of neural activity

Benedetta Mariani^{1,2}, Giorgio Nicoletti¹, Marta Bisio^{2,3}, Marta Maschietto³, Stefano Vassanelli^{2,3}, Samir Suweis^{1,2}

¹*Department of Physics and Astronomy “Galileo Galilei”*

University of Padova, Padova, Italy

²*Padova Neuroscience Center*

University of Padova, Padova, Italy

³*Department of Biomedical Science*

University of Padova, Padova, Italy

The critical brain hypothesis has emerged as an attractive framework to understand the functional implications of the variability in brain activity. However, the mechanisms behind the observed emergent collective neural patterns remain unclear. Here we propose a modeling framework to reconcile apparent contrasting results. We show that the presence of scale-free neuronal avalanches and the associated crackling-noise relation can be explained by the presence of an extrinsic, stochastic-induced mutual information in the system, whereas the intrinsic spatial correlation structure shows the typical features of systems close to their critical point. We test our results on data obtained from the rat’s cortex through state-of-the-art multi-array probes.

The critical brain hypothesis (CBH) has been much investigated since scale-free neuronal avalanches were found in 2003 by Beggs and Plentz [1–9]. In their seminal work they showed that, by analyzing the Local Field Potentials (LFPs) from cortical slices and cultures on chips, cascades of neuronal activity are power-law distributed in their sizes and lifetimes, with exponents remarkably close to the ones of a critical branching process. Since then, such power-laws have been repeatedly observed in experiments [10–15], giving rise to the possibility that the brain might be poised near the critical point of a phase transition. However, the hypothesis is still widely debated [16–23], and reconciling the different views and experimental results remain pressing.

On the one hand, many subsequent works showed that the presence of power-law avalanches is not a sufficient condition for criticality and they might emerge in different contexts [17, 20, 24]. In particular, the authors of [19] found power-law distributed avalanches in models far from a transition region or without any critical transition at all. Remarkably, they also found that the temporal profile of such avalanches collapses into a universal scaling function, as suggested by previous experimental evidences [25]. What is now usually considered the stringest test for criticality is verifying whether the avalanche exponents satisfy the crackling-noise relation [23, 25, 26], which is thought to hold only at criticality [27]. However, very recently it has been pointed out [22] that this relation can be fulfilled even in models of independent spiking units, for a range of choices of the power-law fitting method. Arguably, a more fundamental signature of criticality is the presence of long-range correlations in space [28], which manifest themselves in a correlation length that scales with the system size. Nevertheless, these methods have been applied only at coarser scales, such as in whole brain studies [29, 30], and not in specific cortical areas. The reason is that when neural activity is measured in the form of LFPs through neural probes spatial information is limited due to the poor density of

recording micro-electrodes. When such spatial information is not available, phenomenological renormalization group procedures [31, 32] have been recently proposed as alternatives to test CBH.

On the other hand, the debate about the “nature” of the transition related to the observed brain dynamics is very much open, and thus the class of universality of the critical point from which power-law avalanches might emerge is poorly understood. In particular, recent works have proposed that the observed transition is related to a synchronous-asynchronous one [27, 33, 34] or a disorder-induced transition [30], contrarily to the original, simpler hypothesis of a critical branching process.

All in all, these scattered results call for an unified view of the CBH, allowing to explain the different experimental evidences [23, 35] and elucidate the mechanisms underlying the observed critical signatures of neural activity. In this work, we try to propose such a framework, combining experimental and theoretical approaches.

First, we exploit state of the art spatially-extended multi-arrays to record LFPs from the barrel cortex of anesthetized rats and we look at both the avalanche statistics and the spatial correlations. In order to shed a light on the underlying process from which such collective properties emerge, we develop an analytical framework where we can disentangle the effects of the intrinsic contributions to the neuronal activity - due to the direct interaction between the units themselves - and the extrinsic contributions - arising from externally-driven activity. We will show that by considering both the intrinsic activity, stemming from the reconstructed couplings, and the extrinsic contribution, corresponding to an external stochastic modulation, we are able to understand which collective neural patterns are fundamental in the understanding of the underlying biological mechanisms, and what others simply emerge from stochasticity.

We have measured the population activity in the primary somatosensory cortex of four rats [37]. The cortical activity is recorded through a 256-channels array orga-

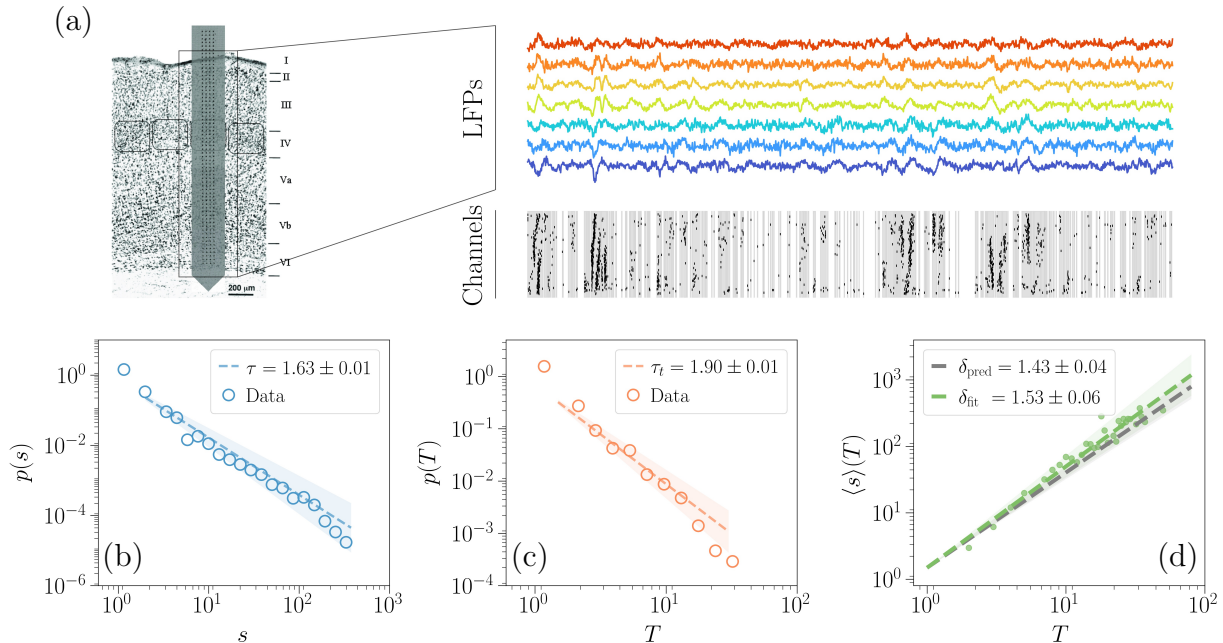


FIG. 1. (a) (Left) Scheme of the array used to obtain the LFPs data from all the cortical layers of the barrel cortex (modified from [36]), (right) an example of the LFPs signals for different layers and the corresponding discretization. An array of 256 channels organized in a 64×4 matrix is inserted in a barrel column and the signals from the cortical layers are collected by 55×4 electrodes. (b-d) Avalanche statistics obtained from the analysis of LFPs data in a rat. Both the distribution of the avalanches (b) sizes and (c) duration are power-laws, and (d) the crackling-noise relation is satisfied.

nized in a 64 rows \times 4 columns matrix with an inter-electrode distance of $32 \mu\text{m}$ [38]. The LFP signal is sampled at 976.56 Hz and band-pass filtered at 2 - 300 Hz [37]. An example of the recorded signals is shown in Figure 1a. We first look at the statistics of the size and the duration of neuronal avalanches. The avalanche statistics is analyzed in LFPs data following standardized pipelines for event detection [10, 13, 39] and the avalanche definition [1]. In particular, the data are temporally binned, avalanches are defined as sequences of bins that present activity, and an avalanche ends once an empty bin is found - the temporal bin chosen is the average inter-event interval, as it is typically done in avalanche analysis [1].

Then, the distribution $p(s)$ of the avalanches sizes - the number of events in each avalanche - and of the avalanche duration $p(T)$ are computed and fitted using a corrected maximum likelihood method [35, 40]. We find that both are statistically compatible with the expected power-laws $P(s) \sim s^{-\tau}$ and $P(T) \sim T^{-\tau_t}$ as we show in Figure 1b-c. Averaging over four rats, we find an inter-rat variability with average exponents $\langle \tau \rangle = 1.75 \pm 0.1$ and $\langle \tau_t \rangle = 2.1 \pm 0.3$ [37]. We also study whether the crackling noise relation $\delta_{\text{pred}} = \frac{\tau_t - 1}{\tau - 1}$ among the exponents [26] is verified, by comparing it with δ_{fit} obtained by fitting the relation $\langle s \rangle(T) \sim T^{\delta_{\text{fit}}}$. Indeed, as in Figure 1d and for each of our rats, the crackling-noise relation holds with an average exponent $\langle \delta_{\text{pred}} \rangle = 1.47 \pm 0.18$ that is indeed compatible with $\langle \delta_{\text{fit}} \rangle = 1.46 \pm 0.04$. However, in spite of the fact that this relation is typically considered one of the stringest test for criticality, we will show that it can

be solely explained by a non-critical dynamics modulated by an heterogeneous shared input.

Experimental data from neural activity are the result of an extremely complex set of underlying interactions, which are often quite difficult to disentangle. In principle, however, it might be interesting to divide them into two very general categories [41, 42]: *intrinsic activity*, which is the activity driven by interactions between neurons or populations of neurons; and *extrinsic activity*, which instead corresponds to the activity modulated by an external or global input. In our case, the intrinsic activity is the result of the propagation dynamics across the multi-layer network of the interconnected neurons along the barrel, whereas the extrinsic activity is given by the external inputs triggering or modulating the propagation (e.g. synaptic current injection from the thalamic inputs). We now present a framework where we can disentangle these two contributions to the overall barrel neural activity, which is the only one that can be actually measured experimentally.

We introduce a model of N variables (v_1, \dots, v_N) , denoting the activity of N units (e.g. neurons or distinct populations of neurons). Focusing first on the extrinsic activity, we assume that at each time the activities are conditionally independent given the state of an external input. In particular, let us now consider a specific neural dynamics and model the evolution of the $\{v_i\}$ through an Ornstein-Uhlenbeck (OU) process [43, 44] of the form

$$\frac{dv_i(t)}{dt} = -\frac{1}{\gamma_i} v_i(t) + \sqrt{D(t)} \eta_i(t) \quad (1)$$

where γ_i is the characteristic time of the i -th neuron and $\eta_i(t)$ is a white noise with a time-dependent amplitude $\mathcal{D}(t)$, which simply corresponds to a noise modulation from an external input that is shared among all the units. In particular, we define the noise modulation in terms of an auxiliary variable $D(t)$,

$$\mathcal{D}(t) = \begin{cases} \mathcal{D}^* & \text{if } D(t) \leq \mathcal{D}^* \\ D(t) & \text{if } D(t) > \mathcal{D}^* \end{cases} \quad (2)$$

where $D(t)$ is itself an OU process [19] with characteristic time γ_D and constant diffusion coefficient θ [45]

$$\frac{dD(t)}{dt} = -\frac{1}{\gamma_D}D(t) + \sqrt{\theta}\eta_D(t). \quad (3)$$

Intuitively, the noise modulation \mathcal{D} can be either constant in time and equal to \mathcal{D}^* or change in time according to an OU process with value $D(t) > \mathcal{D}^*$. Hence, \mathcal{D}^* is the smallest possible noise amplitude of the units, which is maintained for arbitrarily long periods of time.

We now assume that the timescales of the two processes are separable, that is $\gamma_D \gg \gamma_i$. Loosely speaking, this is the limit in which $\mathcal{D}(t)$ is locally constant in time with respect to v_i . In this limit we can effectively write the stationary probability distribution of the activity given the extrinsic activity alone as $p(v) = \int d\mathcal{D} \prod_{i=1}^N p(v_i|\mathcal{D})p(\mathcal{D})$. This is what we have typically access to in experiments, since the states of the external sources are not known in general.

The interesting feature of these kind of models is that we can usually write down joint probability distributions explicitly [37]. In particular we can write the joint probability of two activities as

$$p(v_i, v_j) = \frac{1 + \text{Erf}\left(\frac{\mathcal{D}^*}{\sqrt{\theta\gamma_D}}\right)}{2\pi\mathcal{D}^* \sqrt{\gamma_i\gamma_j}} e^{-\frac{1}{\mathcal{D}^*}\left(\frac{v_i^2}{\gamma_i} + \frac{v_j^2}{\gamma_j}\right)} + \frac{1}{\sqrt{\gamma_i\gamma_j\gamma_D\pi^3\theta}} \int_{\mathcal{D}^*}^{\infty} \frac{d\mathcal{D}}{\mathcal{D}} e^{-\frac{1}{\mathcal{D}}\left(\frac{v_i^2}{\gamma_i} + \frac{v_j^2}{\gamma_j}\right)} e^{-\frac{\mathcal{D}^2}{\theta\gamma_D}}. \quad (4)$$

From this expression it is clear that in general, due to the marginalization over \mathcal{D} , the units are not independent, i.e. $p(v_i, v_j) \neq p(v_i)p(v_j)$. Thus, the presence of a hidden global parameter \mathcal{D} results in the emergence of an effective dependence between the units. To be more precise, a non-vanishing mutual information [46] between v_i and v_j emerges, which is defined as

$$I = \int_{-\infty}^{+\infty} dv_i \int_{-\infty}^{+\infty} dv_j p(v_i, v_j) \log \frac{p(v_i, v_j)}{p(v_i)p(v_j)} \quad (5)$$

and thus captures the whole dependence between v_i and v_j in terms of the factorizability of the related joint probability distribution.

We first highlight that, although the units are not independent, in this particular settings the units are uncorrelated $\langle v_i v_j \rangle - \langle v_i \rangle \langle v_j \rangle = 0 \quad \forall i \neq j$. Second, we

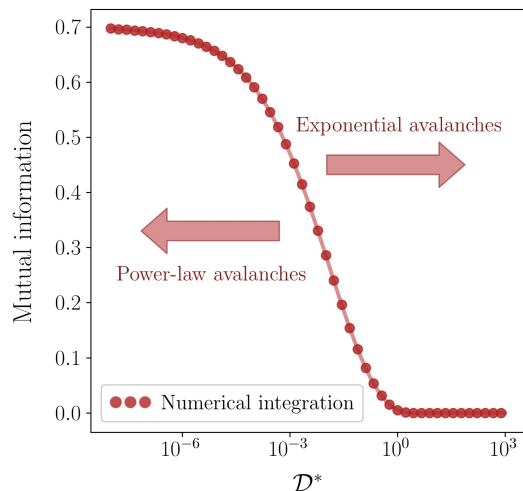


FIG. 2. **The mutual information in the extrinsic model** as a function of \mathcal{D}^* ($\theta = 1$, $\gamma_D = 10$, $\gamma_i = 0.1$, $\gamma_j = 0.5$), obtained from the numerical integration of the Kullback-Leibler divergence between the joint probability distribution in Eq. (4) and its factorization. The onset of a non-vanishing mutual information induced by $\mathcal{D}(t)$, i.e. the onset of the modulation-induced dependence, is also the onset of power-law distributed avalanches.

notice that the parameter \mathcal{D}^* plays a fundamental role in the dynamical evolution of the system. Indeed, if \mathcal{D}^* is high enough the modulation is rare, the units are always dominated by noise and the dynamical evolution is quite trivial (as we can see in Figure 3f). On the other hand, suppose now that \mathcal{D}^* is very small. Whenever $\mathcal{D}(t) = \mathcal{D}^*$ the noise contribution to the units will be very small as well, and their activity will follow an exponential decay. Therefore, in this regime, each v_i will typically alternate periods of quasi-silence to periods of noise-driven activity (corresponding to $\mathcal{D}(t) > \mathcal{D}^*$). Thus, depending on the value of \mathcal{D}^* , this model can either reproduce a noise-driven behavior or a bursty, coordinated one, as shown in Figure 3a. Effectively, we can think about \mathcal{D}^* as a control parameter.

This fact is precisely captured by the emergence of a mutual information between each pair of units in the low \mathcal{D}^* limit. Although Eq. (5) lacks an analytical expression, we can integrate it numerically at different values of our control-like parameter \mathcal{D}^* . The result, in Figure 2, shows that the onset of the coordinated behavior between the units is also the onset of a non-vanishing mutual information among them, which captures a dependence in the system that goes well beyond simple correlations. Interestingly enough, this is also the onset of power-law distributed avalanches of the neural activity.

We simulate the model both in the low \mathcal{D}^* regime and in the high \mathcal{D}^* one, and we perform the same analysis as in the LFP data by detecting events as the points of maximum excursion over a threshold of 2 standard deviations [39]. We find that, as we decrease our control-

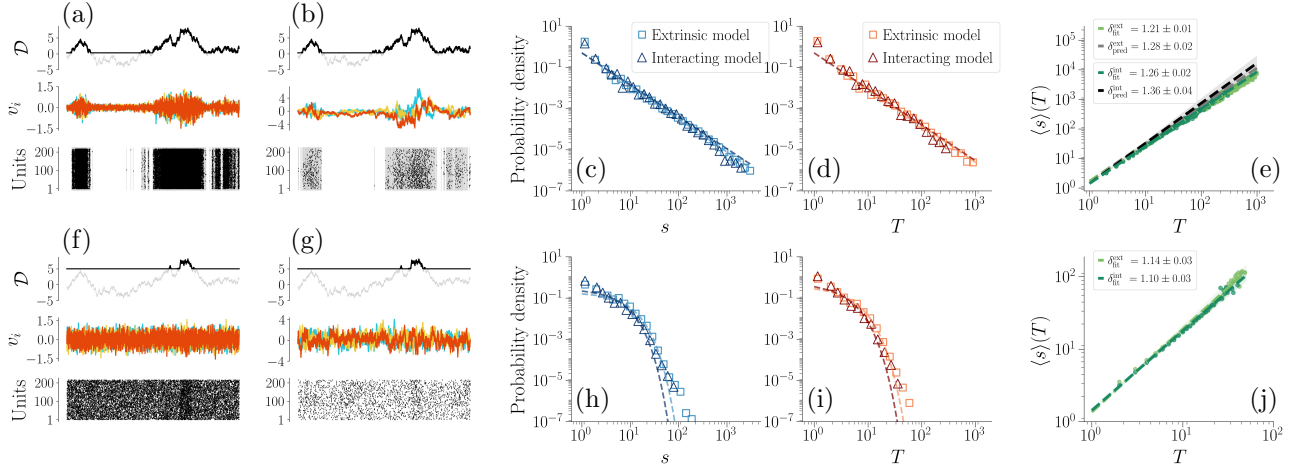


FIG. 3. **Avalanche statistics generated by the model at $\mathcal{D}^* = 0.3$ (a-e) and at $\mathcal{D}^* = 5$ (f-j).** The other parameters are $\gamma_D = 15$ and $\theta = 1$; for the extrinsic model, $\gamma_i = \gamma = 0.05$. (a-b) Comparison between the trajectories of $\mathcal{D}(t)$, v_i and the corresponding discretization in the low- \mathcal{D}^* for the extrinsic model (a) and the interacting one (b). (c-d) In both avalanches are power-law distributed with almost identical exponents. The size distributions have exponents $\tau^{\text{ext}} = 1.60 \pm 0.01$ and $\tau^{\text{int}} = 1.55 \pm 0.01$, whereas the duration distributions have exponents $\tau_t^{\text{ext}} = 1.77 \pm 0.01$ and $\tau_t^{\text{int}} = 1.74 \pm 0.01$. (e) The crackling-noise relation is verified in both cases. In the extrinsic model, we fit an exponent $\delta_{\text{fit}}^{\text{ext}} = 1.21 \pm 0.01$ and from the avalanches exponents we expect $\delta_{\text{pred}}^{\text{ext}} = 1.28 \pm 0.02$. Similarly, in the interacting model we fit an exponent $\delta_{\text{fit}}^{\text{int}} = 1.26 \pm 0.02$ and we expect $\delta_{\text{pred}}^{\text{int}} = 1.36 \pm 0.04$. (f-j) Same plots, now in the high- \mathcal{D}^* regime. (f-g) Notice how the noise modulation gradually disappears and so do the temporal bursts in the discretized system. (h-i) Avalanches are now fitted with an exponential distribution. Notice that larger events, corresponding to periods in which $\mathcal{D}(t) > \mathcal{D}^*$, show up in the distributions' tails, suggesting that the shift between exponentials and power-laws is smooth. (j) The average avalanche size as a function of the duration scales with an exponent that, as \mathcal{D}^* increases, becomes closer to the trivial one $\delta_{\text{fit}}^{\text{ext}} \approx \delta_{\text{fit}}^{\text{int}} \approx 1$.

like parameter \mathcal{D}^* , a transition appears between non-critical, exponential decaying avalanches and power-law distributed ones, with exponents that are similar to the ones observed in the data [47]. Figures 3c-d-e shows that for \mathcal{D}^* small enough, the stochastic modulation produces scale-free avalanches in both size and time with exponents $\tau^{\text{ext}} = 1.60 \pm 0.01$ and $\tau_t^{\text{ext}} = 1.77 \pm 0.01$ satisfying the crackling-noise relation, i.e. $\delta_{\text{fit}}^{\text{ext}} = 1.21 \pm 0.01 \approx \delta_{\text{pred}}^{\text{ext}} = 1.28 \pm 0.02$. We also note that, as expected from theory of critical phenomena [25], if we rescale avalanches to collapse different temporal profiles onto a single scaling function, the best collapse [48] is obtained with an exponent δ_{col} that is close to $\delta_{\text{fit}}^{\text{ext}}$ and $\delta_{\text{pred}}^{\text{ext}}$ in Figure 3e-j [37]. On the other hand, for higher \mathcal{D}^* only exponential-decaying avalanches are present as we see in Figures 3h-i-j.

We now extend our model by introducing an “intrinsic” component for the dynamics of v_i , allowing for direct interactions among units and richer patterns of activity. We describe the intrinsic activity by a linearized version of a noisy neural network of the Wilson-Cowan type [49], thus adding an interaction network to Eqs. (1-2). Namely, we have

$$\frac{dv_i(t)}{dt} = -\frac{1}{\gamma_i}v_i(t) + \sum_j W_{ij}v_j(t) + \sqrt{\mathcal{D}(t)}\eta_i(t) \quad (6)$$

where W_{ij} is the connectivity matrix describing the interaction between the i -th and the j -th unit. We infer the values of W_{ij} and of γ_i directly from the data by

solving the related inverse problem, in such a way that the correlations of the model - which were vanishing in the extrinsic part - match the experimentally-measured correlations σ_{ij} of our LFPs. In order to find the appropriate W_{ij} , we need to solve the following Lyapunov equation for the symmetric matrix A , i.e.

$$\sum_k [\sigma_{ik}A_{kj} + A_{ik}\sigma_{kj}] = \delta_{ij} \int_{\mathcal{D}^*}^{\infty} \mathcal{D} p(\mathcal{D}) d\mathcal{D}, \quad (7)$$

and the inferred interactions are given by [37] $W_{ij} = \delta_{ij}/\gamma_i - A_{ij}$, where δ_{ij} is the Kronecker delta and $\gamma_i = A_{ii}$. The different regimes for the interacting model are plotted in Figures 3f-g.

We now ask whether adding the intrinsic activity in the neural dynamics affects the overall avalanche statistics. As shown in Figures 3c-d-e, all avalanches exponents $\tau \approx 1.6$, $\tau_t \approx 1.75$ and $\delta \approx 1.28$ are not significantly changed by the inclusion of the direct interaction among the units, and in Figures 3h-i-j we see that the high \mathcal{D}^* regime is not changed either. Let us note that these exponents are different from the ones obtained in LFP data, but this is perhaps not surprising. In fact, besides the fact that we observe a non negligible variability in the exponents of LFP signals, we do expect the exponents to change across individuals, and to depend on the particular choice of the extrinsic modulation [50]. Recent findings [23, 50] suggest that τ and τ_t themselves vary along different experimental settings, but they lay along a scaling line such that $\delta \approx 1.28$. This latter exponent

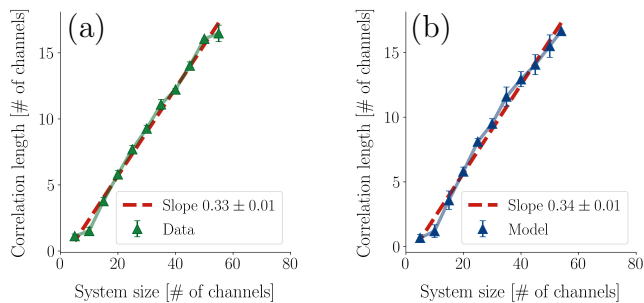


FIG. 4. **Scaling of the correlation length with the system size** in LFPs data (a) and in the interacting model (b). In (a) the average is over the four different rats and the error bars are shown as 5 standard deviations from the mean for visual ease. Both in the data and in the model the correlation length scales linearly with the system size with no plateau in sight, a hallmark of criticality.

is the one reproduced by our model. Notice that we do find this exponent in our experimental setting if we look at spikes data rather than LFPs [35], that is known to be more suitable for studying the crackling-noise relation [25].

At the same time, the fact that the exponents do not change when we add the interaction network to our model has a very profound implication: if we measure neural avalanches alone we cannot infer anything on the intrinsic neural dynamics of our model. However, it is the intrinsic dynamics that determines a non-trivial correlation structure of the model. We thus want to investigate whether the correlations of the measured LFP activity and of our model display any signature of criticality [29, 51]. In particular, we study the scaling of the correlation length ξ , measured as the average distance at which the correlations of the fluctuations around the mean cross zero [52], as a function of the system's sizes L [37]. At the critical point, we expect that the correlation length diverges in the thermodynamic limit [28] and thus in a finite system it should grow with its size - that is, system-spanning correlations are present. Indeed, as shown in Figures 4a-b, we find that both in the data and in the interacting model ξ scales linearly with L . This strongly suggests that the intrinsic interactions are at the root of the critical behavior of the reconstructed system, whereas it is the extrinsic component that is responsible for the emergence of power-law avalanches.

In this work we have shown that while power-law avalanches and the crackling-noise relation appear in LFP data obtained through a multi-array probe from the rat's barrel cortex, their relation with criticality is far from stringent. In order to shed a light on the underlying process from which such collective properties emerge, we have developed an analytically tractable framework where the intrinsic contributions to the neuronal activity, due to the direct interaction between the units themselves, and the extrinsic ones, arising from externally-driven modulated activity, are exactly disentangled. The

latter has been modeled through an approach that is similar to a superstatistics [53] and we have shown that it is able to switch to a regime where avalanches are power-law distributed and satisfy the crackling-noise relation, compatible with the apparently super-universal exponents characterizing the experiments highlighted in [23].

This strongly suggests that external modulation can be on itself a general mechanism behind the emergence of power-law avalanches, as previously reported for less general models [19]. To our knowledge, avalanches distributed with all the exponents of the critical branching process - once properly taking into account the role of gamma-oscillations and of sampling effects [54] - were only found experimentally in [55]. On the other hand, the much wider set of experimental results proposed in [23] suggests that power-law neuronal avalanches share the exponent $\delta \approx 1.28$. The fact that this exponent turns out to be so ubiquitous in a variety of neural systems, from freely moving or anesthetized mammals to ex-vivo preparations of the turtle's nervous system or cultured slice, suggests that it could be explained by some basic phenomena shared by all these systems [22]. We propose that such phenomena can be represented by a simple time varying extrinsic dynamics, that does not require any fine tuning to criticality.

In particular, our model incorporates a control-like parameter, \mathcal{D}^* , whose value directly determines the presence of power-law avalanches in the absence of an underlying direct interaction. To be precise, \mathcal{D}^* controls in a smooth fashion the factorizability of the joint probability distributions of the extrinsic model and thus it is directly related to the presence of a non-vanishing mutual information. Our modeling approach allows us to combine this extrinsic dynamics to an intrinsic one, described by an interaction matrix inferred directly from the experimental data. Once these intrinsic interactions are taken into account, typical signatures of critical systems - such as the scaling of the correlation length with the system size - appear. While they can coexist with phenomena like power-law avalanches, these kind of signatures cannot be possibly explained by the extrinsic activity alone and thus are much more deeply related to the CBH. Indeed, it is not hard to imagine that properties such as scale-free spatial correlations may play a fundamental role in the advantages that the brain might achieve by being critical [3, 9, 56, 57]. Hence, by considering both the intrinsic activity and the extrinsic contributions, our work sheds a light on which critical signatures of neural activity are fundamental in the understanding of the underlying biological mechanisms, and what others are simply the signatures of a stochastic-induced collective dynamics.

ACKNOWLEDGMENTS

S.S. acknowledges DFA and UNIPD for *SUWE_BIRD2020_01* grant, and INFN for LIN-

COLN grant. S.V acknowledges support from the Europea Commission, FET Proactive, SYNCH project (GA number 824162).

-
- [1] J. M. Beggs and D. Plenz, “Neuronal avalanches in neocortical circuits,” *Journal of Neuroscience*, vol. 12, p. 23(35):11167–11177, 2003.
- [2] L. de Arcangelis, C. Perrone-Capano, and H. J. Herrmann, “Self-organized criticality model for brain plasticity,” *Physical Review Letters*, vol. 96, no. 2, p. 028107, 2006.
- [3] O. Kinouchi and M. Copelli, “Optimal dynamical range of excitable networks at criticality,” *Nature physics*, vol. 2, no. 5, pp. 348–351, 2006.
- [4] W. L. Shew and D. Plenz, “The functional benefits of criticality in the cortex,” *The Neuroscientist*, vol. 19,1, pp. 88–100, 2013.
- [5] J. Hesse and T. Gross, “Self-organized criticality as a fundamental property of neural systems,” *Frontiers in systems neuroscience*, vol. 8, p. 166, 2014.
- [6] G. Tkačik, T. Mora, O. Marre, D. Amodei, S. E. Palmer, M. J. Berry, and W. Bialek, “Thermodynamics and signatures of criticality in a network of neurons,” *Proceedings of the National Academy of Sciences*, vol. 112, no. 37, pp. 11508–11513, 2015.
- [7] R. P. Rocha, L. Koçillari, S. Suweis, M. Corbetta, and A. Maritan, “Homeostatic plasticity and emergence of functional networks in a whole-brain model at criticality,” *Scientific reports*, vol. 8, no. 1, pp. 1–15, 2018.
- [8] J. Hidalgo, J. Grilli, S. Suweis, M. A. Munoz, J. R. Banavar, and A. Maritan, “Information-based fitness and the emergence of criticality in living systems,” *Proceedings of the National Academy of Sciences*, vol. 111, no. 28, pp. 10095–10100, 2014.
- [9] M. A. Muñoz, “Colloquium: Criticality and dynamical scaling in living systems,” *Review of Modern Physics*, vol. 90, p. 031001, 2018.
- [10] T. Petermann, T. C. Thiagarajan, M. A. Lebedev, M. A. L. Nicolelis, D. R. Chialvo, and D. Plenz, “Spontaneous cortical activity in awake monkeys composed of neuronal avalanches,” *Proceedings of the National Academy of Sciences*, vol. 106, no. 37, pp. 15921–15926, 2009.
- [11] S. Yu, H. Yang, H. Nakahara, G. S. Santos, D. Nikolić, and D. Plenz, “Higher-order interactions characterized in cortical activity,” *Journal of Neuroscience*, vol. 31, no. 48, pp. 17514–17526, 2011.
- [12] G. Hahn, T. Petermann, M. Havenith, and al., “Neuronal avalanches in spontaneous activity in vivo,” *Journal of Neurophysiology*, vol. 104(6), p. 3312–3322, 2010.
- [13] E. D. Gireesh and D. Plenz, “Neuronal avalanches organize as nested theta- and beta/gamma-oscillations during development of cortical layer 2/3,” *Proceedings of the National Academy of Sciences*, p. 7576–7581, 2008.
- [14] A. Mazzoni, F. D. Broccard, E. Garcia-Perez, P. Bonifazi, M. Ruaro, and V. Torre, “On the dynamics of the spontaneous activity in neuronal networks,” *PLoS One*, vol. 2(5):e439, 2007.
- [15] V. Pasquale, P. Massobrio, L. Bologna, M. Chiappalone, and S. Martinoia, “Self-organization and neuronal avalanches in networks of dissociated cortical neurons,” *Neuroscience*, vol. 153(4), p. 1354–1369, 2008.
- [16] C. Bedard, H. Kroeger, and A. Destexhe, “Does the 1/f frequency scaling of brain signals reflect self-organized critical states?,” *Physical Review Letters*, vol. 97, no. 11, p. 118102, 2006.
- [17] J. Touboul and A. Destexhe, “Can power-law scaling and neuronal avalanches arise from stochastic dynamics?,” *PLOS ONE*, vol. 5, pp. 1–14, 02 2010.
- [18] J. M. Beggs and N. Timme, “Being critical of criticality in the brain,” *Frontiers in physiology*, vol. 3, p. 163, 2012.
- [19] J. Touboul and A. Destexhe, “Power-law statistics and universal scaling in the absence of criticality,” *Physical Review E*, vol. 95, p. 012413, 2017.
- [20] M. Martinello, J. Hidalgo, A. Maritan, S. di Santo, D. Plenz, and M. A. Muñoz, “Neutral theory and scale-free neural dynamics,” *Physical Review X*, vol. 7, p. 041071, 2017.
- [21] J. Wilting and V. Priesemann, “25 years of criticality in neuroscience — established results, open controversies, novel concepts,” *Current Opinion in Neurobiology*, vol. 58, pp. 105 – 111, 2019.
- [22] A. Destexhe and J. D. Touboul, “Is there sufficient evidence for criticality in cortical systems?,” *eNeuro*, vol. 8, no. 2, 2021.
- [23] A. J. Fontenele, N. A. P. de Vasconcelos, T. Feliciano, L. A. A. Aguiar, C. Soares-Cunha, B. Coimbra, L. Dalla Porta, S. Ribeiro, A. J. a. Rodrigues, N. Sousa, P. V. Carelli, and M. Copelli, “Criticality between cortical states,” *Physical Review Letters*, vol. 122, p. 208101, 2019.
- [24] A. Faqeeh, S. Osat, F. Radicchi, and J. P. Gleeson, “Emergence of power laws in noncritical neuronal systems,” *Physical Review E*, vol. 100, no. 1, p. 010401, 2019.
- [25] N. Friedman, S. Ito, B. A. W. Brinkman, M. Shimono, R. E. L. DeVille, K. A. Dahmen, J. M. Beggs, and T. C. Butler, “Universal critical dynamics in high resolution neuronal avalanche data,” *Physical Review Letters*, vol. 108, p. 208102, 2012.
- [26] J. Sethna, K. Dahmen., and C. Myers, “Crackling noise,” *Nature*, vol. 410, p. 242–250, 2001.
- [27] S. di Santo, P. Villegas, R. Burioni, and M. A. Muñoz, “Simple unified view of branching process statistics: Random walks in balanced logarithmic potentials,” *Physical Review E*, vol. 95, p. 032115, 2017.
- [28] J. J. Binney, N. J. Dowrick, A. J. Fisher, and M. Newman, *The Theory of Critical Phenomena: An Introduction to the Renormalization Group*. USA: Oxford University Press, Inc., 1992.
- [29] A. Haimovici, E. Tagliazucchi, P. Balenzuela, and D. R. Chialvo, “Brain organization into resting state networks emerges at criticality on a model of the human connec-

- to me,” *Physical Review Letters*, vol. 110, p. 178101, 2013.
- [30] A. Ponce-Alvarez, A. Jouary, M. Privat, G. Deco, and G. Sumbre, “Whole-brain neuronal activity displays crackling noise dynamics,” *Neuron*, vol. 100, no. 6, pp. 1446 – 1459.e6, 2018.
- [31] L. Meshulam, J. L. Gauthier, C. D. Brody, D. W. Tank, and W. Bialek, “Coarse graining, fixed points, and scaling in a large population of neurons,” *Physical Review Letters*, vol. 123, no. 17, p. 178103, 2019.
- [32] G. Nicoletti, S. Suweis, and A. Maritan, “Scaling and criticality in a phenomenological renormalization group,” *Physical Review Research*, vol. 2, p. 023144, 2020.
- [33] L. Dalla Porta and M. Copelli, “Modeling neuronal avalanches and long-range temporal correlations at the emergence of collective oscillations: Continuously varying exponents mimic M/EEG results,” *PLOS Computational Biology*, vol. 15, no. 4, pp. 1–26, 2019.
- [34] S. S. Poil, R. Hardstone, H. D. Mansvelder, and K. Linkenkaer-Hansen, “Critical-state dynamics of avalanches and oscillations jointly emerge from balanced excitation/inhibition in neuronal networks,” *Journal of Neuroscience*, vol. 32, no. 29, pp. 9817–9823, 2012.
- [35] B. Mariani, G. Nicoletti, M. Bisio, M. Maschietto, R. Oboe, S. Suweis, and S. Vassanelli, “Beyond resting state neuronal avalanches in the somatosensory barrel cortex,” *bioRxiv*, 2021.
- [36] Z.-W. Zhang and M. Deschênes, “Intracortical axonal projections of lamina vi cells of the primary somatosensory cortex in the rat: A single-cell labeling study,” *Journal of Neuroscience*, vol. 17, no. 16, pp. 6365–6379, 1997.
- [37] See Supplemental Material for experimental details, further statistical analysis, details on the numerical simulations and analytical derivations.
- [38] S. Schröder, C. Cecchetto, S. Keil, M. Mahmud, E. Brose, O. Dogan, G. Bertotti, D. Wolanski, B. Tillack, J. Schneidewind, H. Gargouri, M. Arens, J. Bruns, B. Szyszka, S. Vassanelli, and R. Thewes, “Cmos-compatible purely capacitive interfaces for high-density in-vivo recording from neural tissue,” in *2015 IEEE Biomedical Circuits and Systems Conference (BioCAS)*, pp. 1–4, 2015.
- [39] O. Shriki, J. Alstott, F. Carver, T. Holroyd, R. N. Henson, M. L. Smith, R. Coppola, E. Bullmore, and D. Plenz, “Neuronal avalanches in the resting meg of the human brain,” *Journal of Neuroscience*, vol. 33, no. 16, pp. 7079–7090, 2013.
- [40] M. Gerlach and E. G. Altmann, “Testing statistical laws in complex systems,” *Physical Review Letters*, vol. 122, p. 168301, 2019.
- [41] V. Priesemann and O. Shriki, “Can a time varying external drive give rise to apparent criticality in neural systems?,” *PLoS computational biology*, vol. 14, no. 5, p. e1006081, 2018.
- [42] U. Ferrari, S. Deny, M. Chalk, G. Tkačik, O. Marre, and T. Mora, “Separating intrinsic interactions from extrinsic correlations in a network of sensory neurons,” *Physical Review E*, vol. 98, no. 4, p. 042410, 2018.
- [43] L. M. Ricciardi and L. Sacerdote, “The ornstein-uhlenbeck process as a model for neuronal activity,” *Biological cybernetics*, vol. 35, no. 1, pp. 1–9, 1979.
- [44] H. C. Tuckwell, F. Y. Wan, and J.-P. Rospars, “A spatial stochastic neuronal model with ornstein–uhlenbeck input current,” *Biological cybernetics*, vol. 86, no. 2, pp. 137–145, 2002.
- [45] One can set $\theta = 1$ without loss of generality, hence we often do so to reduce the number of free parameters of the model.
- [46] T. M. Cover and J. A. Thomas, *Elements of Information Theory*. USA: Wiley-Interscience, 2006.
- [47] Let us note that even for high but reasonable values of \mathcal{D}^* some modulation is still present, although it is much rarer. This simple fact is reflected in the presence of non-exponential tails in Figures 3h-i. This strongly suggests that the transition between exponential avalanches and power-law ones is smooth, as it is suggested by the mutual information in Figure 2 which does not show any discontinuity.
- [48] N. Marshall, N. M. Timme, N. Bennett, M. Ripp, E. Lautzenhiser, and J. M. Beggs, “Analysis of power laws, shape collapses, and neural complexity: New techniques and matlab support via the ncc toolbox,” *Frontiers in Physiology*, vol. 7, p. 250, 2016.
- [49] R. F. Galán, “On how network architecture determines the dominant patterns of spontaneous neural activity,” *PLOS ONE*, vol. 3, pp. 1–10, 05 2008.
- [50] L. J. Fosque, R. V. Williams-García, J. M. Beggs, and G. Ortiz, “Evidence for Quasicritical Brain Dynamics,” *Physical Review Letters*, vol. 126, no. 9, p. 098101, 2021.
- [51] D. Fraiman and D. R. Chialvo, “What kind of noise is brain noise: anomalous scaling behavior of the resting brain activity fluctuations,” *Frontiers in Physiology*, vol. 3, p. 307, 2012.
- [52] A. Cavagna, A. Cimarelli, I. Giardina, G. Parisi, R. Santagati, F. Stefanini, and M. Viale, “Scale-free correlations in starling flocks,” *Proceedings of the National Academy of Sciences*, vol. 107, no. 26, pp. 11865–11870, 2010.
- [53] C. Beck and E. Cohen, “Superstatistics,” *Physica A: Statistical Mechanics and its Applications*, vol. 322, pp. 267–275, 2003.
- [54] T. T. A. Carvalho, A. J. Fontenele, M. Girardi-Schappo, T. Feliciano, L. A. A. Aguiar, T. P. L. Silva, N. A. P. de Vasconcelos, P. V. Carelli, and M. Copelli, “Subsampled directed-percolation models explain scaling relations experimentally observed in the brain,” *Frontiers in Neural Circuits*, vol. 14, p. 83, 2021.
- [55] S. R. Miller, S. Yu, and D. Plenz, “The scale-invariant, temporal profile of neuronal avalanches in relation to cortical gamma oscillations,” *Scientific Reports*, vol. 9, 2019.
- [56] W. Bialek and T. Mora, “Are biological systems poised at criticality?,” *Journal of Statistical Physics*, vol. 144, no. 2, 2011.
- [57] D. R. Chialvo, “Emergent complex neural dynamics,” *Nature Physics*, vol. 6, no. 744, 2010.
- [58] P. Kloeden and E. Platen, *Numerical Solution of Differential Stochastic Equations*. Springer Berlin, 1999.
- [59] L. Swanson, *Brain maps: structure of the rat brain*. London, Academic press, third ed., 2003.
- [60] Notice that this is the stationary distribution of the opposite time-scale separation limit, namely $\gamma_D \ll \gamma_i$, for all i . In this limit, the process for \mathcal{D} reaches stationarity much faster than the one for v_i , thus v_i diffuses with a constant effective diffusion coefficient.
- [61] C. W. Gardiner, *Handbook of stochastic methods for physics, chemistry and the natural sciences*, vol. 13 of *Springer Series in Synergetics*. Springer-Verlag, third ed., 2004.
- [62] Let us note that the process is simulated through its discrete version by employing the Euler–Maruyama method

[58], and for this purpose a finite dt has to be chosen. The deterministic part of the discrete version of the process is a discrete map of the form $\mathbf{v}(t + dt) = K\mathbf{v}(t)$, where $K = \mathbb{I} + (W - \frac{\mathbb{I}}{\gamma})dt$. When choosing dt one has to ensure that K has spectral radius less than unity, in order to guarantee stability.

- [63] R. H. Bartels and G. W. Stewart, "Solution of the matrix equation $AX + XB = C$," *Commun. ACM*, vol. 15, no. 9, p. 820–826, 1972.
- [64] T. L. Ribeiro, S. Yu, D. A. Martin, D. Winkowski, P. Kanold, D. R. Chialvo, and D. Plenz, "Trial-by-trial variability in cortical responses exhibits scaling in spatial correlations predicted from critical dynamics," *bioRxiv*, 2020.
- [65] D. A. Martin, T. L. Ribeiro, S. A. Cannas, T. S. Grigera, D. Plenz, and D. R. Chialvo, "Box-scaling as a proxy of finite-size correlations," 2020.
- [66] W. Shew, W. Clawson, J. Pobst, and al, "Adaptation to sensory input tunes visual cortex to criticality.," *Nature Phys.*, vol. 11, p. 659–663, 2015.
- [67] K. Bansal, J. O. Garcia, N. Lauharatanahirun, S. F. Muldoon, P. Sajda, and J. M. Vettel, "Scale-specific dynamics of large-amplitude bursts in eeg capture behaviorally meaningful variability," 2020.
-

Supplemental Material for “On the critical signatures of neural activity”

A. EXPERIMENTAL SETTING

1. Surgical procedures

LFPs recordings are performed on Wistar rats, which are maintained under standard environmental conditions in the animal research facility of the Department of Biomedical Sciences of the University of Padova. All the procedures are approved by the local Animal Care Committee (O.P.B.A.) and the Italian Ministry of Health (authorization number 522/2018-PR). Young adult rats aged 36 to 43 days and weighting between 150 and 200 g are anesthetized with an intra-peritoneal induction mixture of tiletamine-xylazine (2 mg and 1.4 g/100 g body weight, respectively), followed by additional doses (0.5 mg and 0.5 g/100 g body weight) every hour. The anesthesia level is constantly monitored by testing the absence of eye and hind-limb reflexes and whiskers’ spontaneous movements. Each animal is positioned on a stereotaxic apparatus where the head is fixed by teeth- and ear-bars. To expose the cortical area of interest, an anterior-posterior opening in the skin is made in the center of the head and a window in the skull is drilled over the somatosensory barrel cortex at stereotaxic coordinates $-1 \div -4$ AP, $+4 \div +8$ ML referred to bregma [59]. A slit in the meninges is then carefully made with fine forceps at coordinates -2.5 AP, $+6$ ML for the subsequent insertion of the recording probe. As a reference, the depth is set at $0 \mu\text{m}$ when the electrode proximal to the chip tip touches the cortical surface. The neuronal activity is recorded from the entire barrel cortex (from 0 to $-1750 \mu\text{m}$), which is constantly bathed in Krebs’ solution (in mM: NaCl 120, KCl 1.99, NaHCO_3 25.56, KH_2PO_4 136.09, CaCl_2 2, MgSO_4 1.2, glucose 11). An Ag/AgCl electrode bathed in the extracellular solution in proximity of the probe is used as reference.

2. Recordings

LFPs are recorded through a custom-made needle which integrates a high density array, whose electrodes are organized in a 64×4 matrix. The operation principle of the multi-electrode-arrays used to record LFPs is an extended CMOS based EOSFET (Electrolyte Oxide Semiconductor Field Effect Transistor). The recording electrodes are $7.4 \mu\text{m}$ in diameter size and the needle is $300 \mu\text{m}$ in width and 10mm long. The x- and y-pitch (i.e. the distance between adjacent recording sites) are $32 \mu\text{m}$. The multiplexed signals are then digitized by a NI PXIe-6358 (National Instruments) up to 1.25MS/s at 16bit resolution and saved to disk by a custom LabVIEW acquisition software. The LFP signal is sampled at 976.56 Hz and band-pass filtered ($2\text{-}300 \text{ Hz}$). The dataset analyzed for this work consist in 20 trials of basal activity lasting 7.22 seconds, that are recorded from 4 rats.

3. Barrel cortex

The barrel cortex is the region of the primary somatosensory cortex (S1) that encodes tactile sensory inputs from the rodents’ whiskers. The barrel presents a high degree of segmentation into vertical columns and horizontal layers. The whisker-related barrel column is a cylindrical structure spanning vertically the six layers of the barrel cortex, although its border is defined exclusively by spatially aligned sub-cellular structures in layer 4 called barrels.

Each barrel-column is composed of an archetypal circuit that is repeated in each column. Importantly, the barrels are laid out in a pattern that is nearly identical to the whiskers on the rat’s snout that, together with the underlying neural circuit, suggests a highly specific correspondence between whiskers and barrel columns.

B. THE EXTRINSIC MODEL

As explained in the main text, we introduce a model of N variables (v_1, \dots, v_N) that are conditionally independent given the state of the external input. In particular, let us assume that there are some parameters $\xi = (\xi_1, \dots, \xi_M)$ controlling the extrinsic modulation, that is

$$p(v_i, v_j, t | \xi) = p(v_i, t | \xi) p(v_j, t | \xi) \quad \forall i, j. \quad (\text{S1})$$

Since at this moment we assume no direct interaction is happening, we think about the probability distribution $p(v_i | \xi)$ as shaped by extrinsic activity alone. That is, once we specify ξ , no interaction happens between the i -th variable

and the j -th variable. However, we now suppose that we do not have access on the states of the external parameters. Hence, we can only hope of describing to the joint probability distribution

$$p(v_1, \dots, v_N, t) = \int d\xi \prod_{i=1}^N p(v_i, t | \xi) p(\xi, t) \quad (\text{S2})$$

which is what we typically observe in an experimental setting. In general, due to the marginalization over the external parameters this probability distribution is not factorizable, and thus in this sense it is not trivial.

In general, we want to work in the stationary limit and thus there is a complication we need to take into account. In particular, since the integrand of Equation (S2) can be arbitrarily complicated, we would like to be able to perform the stationary limit before the marginalization, i.e.,

$$\lim_{t \rightarrow \infty} p(v_1, \dots, v_N, t) = \int d\xi \prod_{i=1}^N \lim_{t \rightarrow \infty} p(v_i, t | \xi) \cdot \lim_{t \rightarrow \infty} p(\xi, t).$$

This limit, of course, is not always true, but it does hold if we assume that the time-scales of the two processes - the process for \mathbf{v} and for ξ - are separated. In particular, we are interested in the limit in which the timescale of ξ is slower than \mathbf{v} , so that \mathbf{v} relaxes to its stationary state in a time-frame in which the external modulation can be considered constant.

Let us now describe the particular choices of the main text, where

$$\frac{dv_i(t)}{dt} = -\frac{1}{\gamma_i} v_i(t) + \sqrt{\mathcal{D}(t)} \eta(t) \quad (\text{S3})$$

is the process that generates \mathbf{v} and the single-parameter external modulation is

$$\mathcal{D}(t) = \begin{cases} \mathcal{D}^* & \text{if } D(t) \leq \mathcal{D}^* \\ D(t) & \text{if } D(t) > \mathcal{D}^* \end{cases} \quad (\text{S4})$$

where

$$\frac{dD(t)}{dt} = -\frac{1}{\gamma_D} D(t) + \sqrt{\theta} \eta(t). \quad (\text{S5})$$

For the above considerations to hold, we assume that $\gamma_D \gg \gamma_i$. This is simply a time-scale separation limit. In this limit, the process of v_i reaches stationarity much faster than the process of \mathcal{D} , thus the overall stationary distribution is the stationary distribution $p(v_i | \mathcal{D})$ averaged over the stationary distribution $p(\mathcal{D})$. Hence we have

$$p(\mathcal{D}) = \frac{1}{2} \left[1 + \text{Erf} \left(\frac{\mathcal{D}^*}{\sqrt{\theta} \gamma_D} \right) \right] \delta(\mathcal{D} - \mathcal{D}^*) + \frac{H(\mathcal{D} - \mathcal{D}^*)}{\sqrt{\pi \theta} \gamma_D} e^{-\frac{\mathcal{D}^2}{\theta \gamma_D}}, \quad (\text{S6})$$

where H is the Heaviside step function. Then, the computation of the stationary probability distributions is quite easy. The single-unit probability is given by

$$\begin{aligned} p(v_i) &= \int d\mathcal{D} p(v_i | \mathcal{D}) p(\mathcal{D}) = \int d\mathcal{D} \frac{1}{\sqrt{\pi \gamma_i \mathcal{D}}} e^{-\frac{v_i^2}{\gamma_i \mathcal{D}}} p(\mathcal{D}) \\ &= \frac{1 + \text{Erf} \left(\frac{\mathcal{D}^*}{\sqrt{\theta} \gamma_D} \right)}{2\sqrt{\pi \mathcal{D}^* \gamma_i}} e^{-\frac{v_i^2}{\mathcal{D}^* \gamma_i}} + \frac{1}{\sqrt{\pi^2 \theta \gamma_D \gamma_i}} \int_{\mathcal{D}^*}^{\infty} \frac{d\mathcal{D}}{\sqrt{\mathcal{D}}} e^{-\left[\frac{\mathcal{D}^2}{\theta \gamma_D} + \frac{v_i^2}{\mathcal{D} \gamma_i} \right]} \end{aligned} \quad (\text{S7})$$

and, in principle, we can compute the probability distributions for any number of variables $\{v_i\}$ in the same way.

We note that although before the marginalization the two-point probability distribution is factorizable

$$p(v_i, v_j, \mathcal{D}) = p(v_i, v_j | \mathcal{D}) p(\mathcal{D}) = p(v_i | \mathcal{D}) p(v_j | \mathcal{D}) p(\mathcal{D}),$$

the marginalization itself breaks the factorization, namely

$$\int d\mathcal{D} p(v_i, v_j, \mathcal{D}) \neq \left[\int d\mathcal{D} p(v_i, \mathcal{D}) \right] \left[\int d\mathcal{D} p(v_j, \mathcal{D}) \right].$$

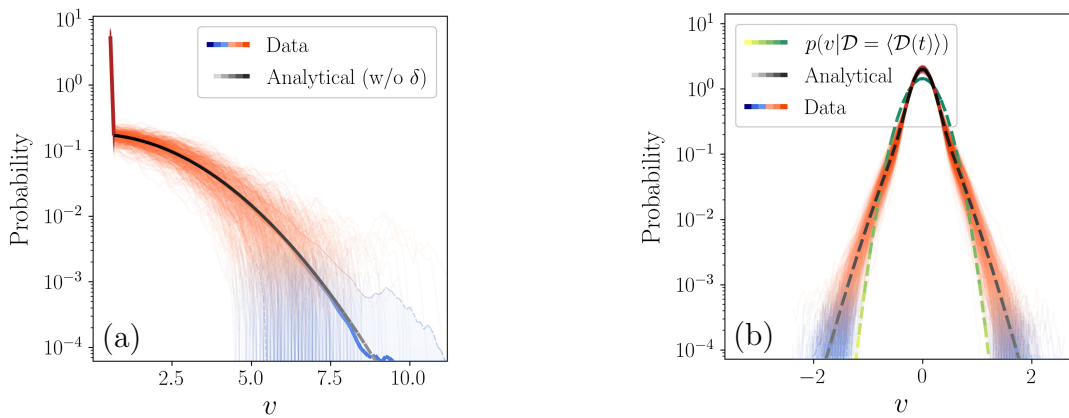


FIG. S1. Comparison between the stationary distributions obtained in the main text and the results 10^3 simulations. Semi-transparent lines represent different simulations. Filled areas of the plots represent one standard deviation from the mean distribution. (a) Probability distribution of \mathcal{D} . (b) Probability distribution of a single v_i .

Hence, we can write down the two-unit joint probability as

$$p(v_i, v_j) = \frac{1 + \text{Erf}\left(\frac{\mathcal{D}^*}{\sqrt{\theta\gamma_D}}\right)}{2\pi\mathcal{D}^*\sqrt{\gamma_i\gamma_j}} e^{-\frac{1}{\mathcal{D}^*}\left(\frac{v_i^2}{\gamma_i} + \frac{v_j^2}{\gamma_j}\right)} + \frac{1}{\sqrt{\gamma_i\gamma_j\gamma_D\pi^3\theta}} \int_{\mathcal{D}^*}^{\infty} \frac{dD}{D} e^{-\frac{1}{D}\left(\frac{v_i^2}{\gamma_i} + \frac{v_j^2}{\gamma_j}\right)} e^{-\frac{D^2}{\theta\gamma_D}} \quad (\text{S8})$$

where the second term is not factorizable.

From these probabilities we can immediately show that

$$\langle v_i v_j \rangle - \langle v_i \rangle \langle v_j \rangle = 0 \quad \forall i \neq j \quad (\text{S9})$$

and, in general, all the expectation values where a variable v_i appears an odd number of times vanish. Let us note that this is not a general feature of these kind of models, but it is rather a property inherited from the choice of an OU process, for which $\int dv_i v_i p(v_i|\mathcal{D}) = 0$ holds. The diagonal entries of the covariance matrix, on the other hand, are given by

$$\langle v_i^2 \rangle = \frac{\gamma_i \mathcal{D}^*}{2} \left[1 + \text{Erf}\left(\frac{\mathcal{D}^*}{\sqrt{\theta\gamma_D}}\right) \right] + \sqrt{\frac{\gamma_i^2 \theta \gamma_D}{16\pi}} e^{-\frac{(\mathcal{D}^*)^2}{\theta\gamma_D}}$$

Thus, in this particular setting, the units are uncorrelated and have a variance that is independent on the other units. At the same time, however, it is clear that in general $p(v_i, v_j) \neq p(v_i)p(v_j)$ so while uncorrelated they are not independent.

C. TESTING THE PREDICTIONS OF THE EXTRINSIC MODEL

We now show that simulations of the extrinsic model described by Equation S3 agree with the analytical results. Whenever not specified, we assume that the parameters of the model are given by $\mathcal{D}^* = 0.3$, $\theta = 1$, $\gamma_D = 10$ together with $\gamma_i = 0.1$, $\gamma_j = 0.5$. Thus, we are in the limit of timescale separation considered in the main text.

Let us begin with Figure S1. Albeit trivial, we first check in Figure S1a that the stationary distribution of \mathcal{D} is indeed the one of Eq. (S6) and in Figure S1b that the stationary distribution of a single v_i does correspond to the analytical expression of Eq. (S7). If we compare this distribution to a standard distribution of an Ornstein-Uhlenbeck process with a diffusion coefficient equal to the mean $\langle \mathcal{D}(t) \rangle$ [60] we immediately see that the distribution of our model is considerably more peaked around zero and displays longer tails. Indeed, one expects that due to the fact that $\mathcal{D}^* < \langle \mathcal{D}(t) \rangle$ the system tends to wander more easily close to zero, especially in the time windows where the diffusion coefficient is constant and equal to \mathcal{D}^* . At the same time, the fact that $\mathcal{D}(t)$ can change in time favors the presence of values of v that are larger in absolute value, which is the mechanism at the origin of the bursty behavior seen in the main text.

In Figure S2 we look instead at the properties of the joint probability distribution $p(v_i, v_j)$. The most natural quantity to compare this distribution with is its factorization $p(v_i)p(v_j)$, which is equivalent to ignoring the feedback

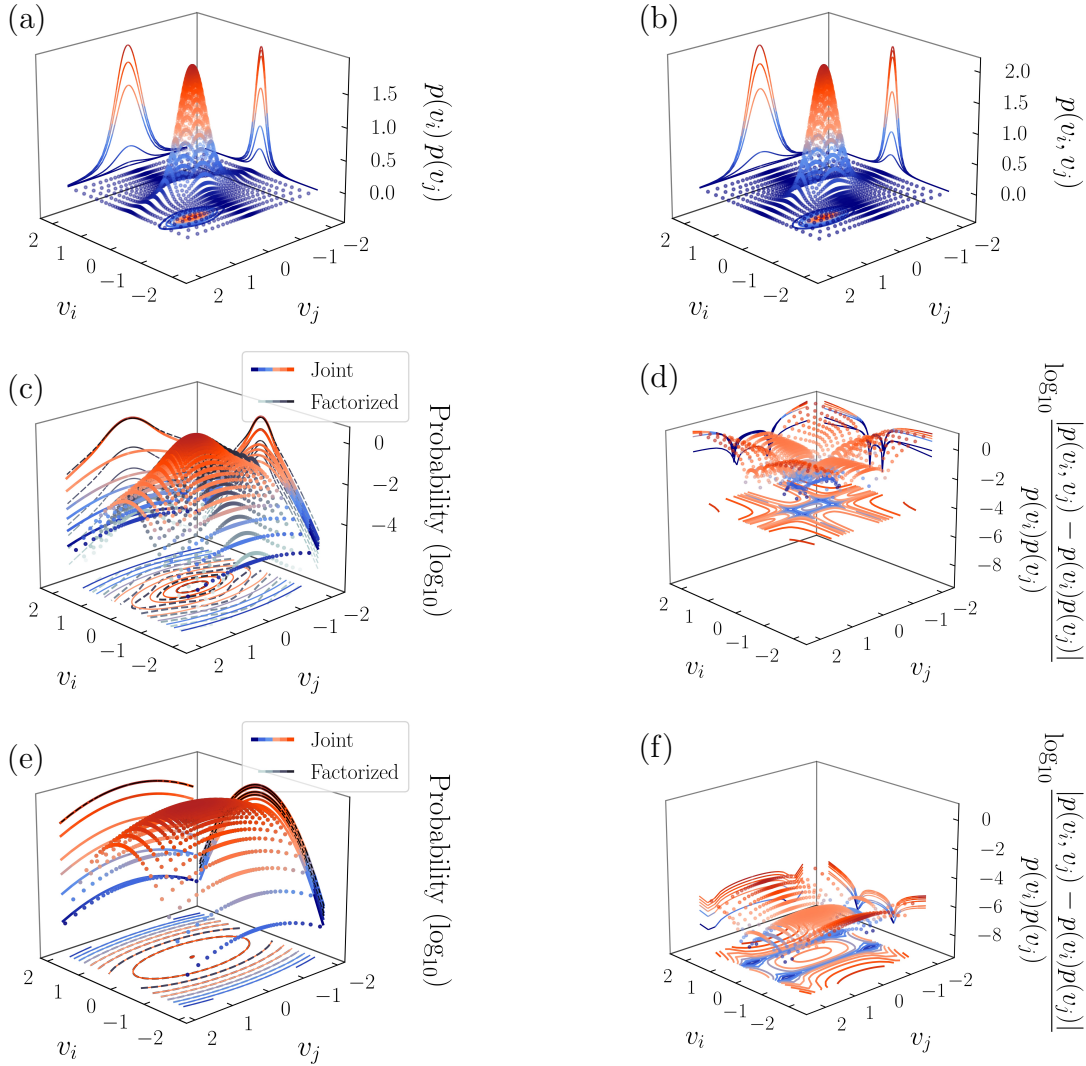


FIG. S2. Comparison between the analytical expressions of the joint probability distribution in Eq. (S8) and its factorization $p(v_i, v_j)$. (a) The factorized distribution. (b) The joint distribution. (c) Comparison between the two in a log-plot. (d) Relative difference between the two with respect to the factorized distribution. (e-f) Comparison between the joint and the factorized distributions, with the same parameters except for $\mathcal{D}^* = 5$.

effects between v_i and v_j due to the shared extrinsic modulation of $\mathcal{D}(t)$. Since we are setting $\mathcal{D}^* = 0.5$, we expect that these effects are going to be particularly relevant for the dynamics of the model. In particular, in Figure S2c-d we see that the most important differences between the two occur in the tails of the two-dimensional distribution, with the joint distribution typically showing dramatically longer tails. This translates to the fact that far-from-zero values of the two variables can occur more easily at the same time.

The situation is completely reversed when we increase \mathcal{D}^* . In Figure S2e-f we see that for $\mathcal{D}^* = 8$ the joint probability distribution and the factorized distribution are almost indistinguishable. Hence, this example shows explicitly that if \mathcal{D}^* is high enough the dependence induced by the extrinsic modulation vanishes.

Let us keep focusing on the case $\mathcal{D}^* = 0.5$ for the time being. In Figure S3a-d we compare the one-dimensional sections of the analytical expression of the joint probability distribution with the results of 10^3 simulations of the model, together with the sections of the factorized distribution. The joint distribution estimated from the simulation matches particularly well the analytical prediction. Once more, and perhaps more clearly, in Figure S3a-b we see the stark difference that emerges along the tails between the joint probability distribution and its factorization. Interestingly, panel (c) and panel (d) show that the situation in the bulk of the distribution is reversed with respect to the tails and now the joint probability distribution is more peaked with respect to its factorization, albeit only slightly. That is, the modulation in the low \mathcal{D}^* regime favors both large values of v_i and v_j and values very close to zero.

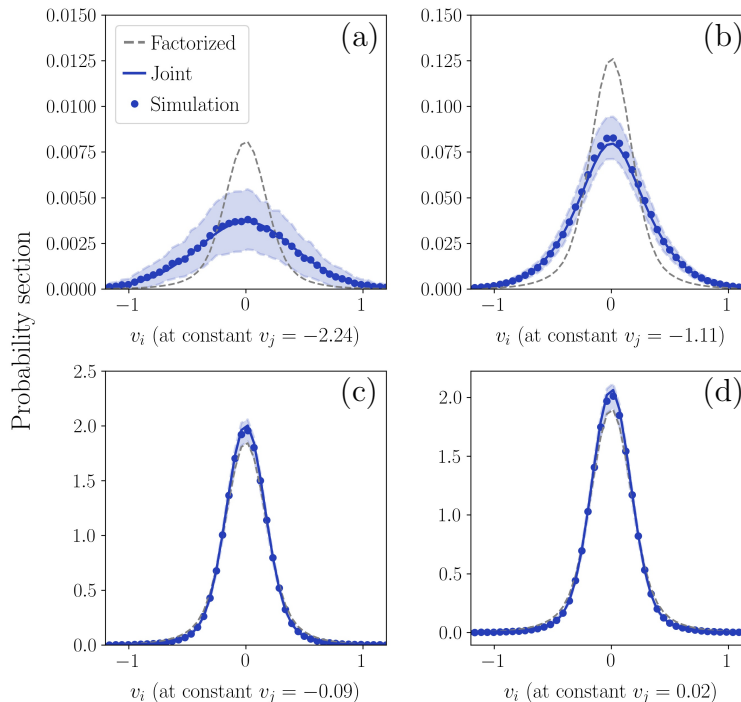


FIG. S3. Comparison between the analytical expressions of the joint probability distribution $p(v_i, v_j)$ given by Eq. (S8) and the one obtained from with 10^3 simulations. We also show the corresponding results for the factorized probabilities. The blue line corresponds to the analytical expression of $p(v_i, v_j)$. The corresponding dots represent the histogram of the distribution obtained from 10^3 simulations, and the semitransparent filled areas represent one standard deviation from this estimate. Similarly, the gray dashed line represent the analytical expression of $p(v_i)p(v_j)$. (a) Section along the v_j direction for small v_j , so that we are looking at the tails of the distribution. Even though the estimate along the tails is noisy, we clearly see that the estimate from the simulations lies along the analytical prediction. (b) As before, but for higher v_j . (c-d) As before, but with values of v_j close to zero so we look at the bulk of the distribution near its peak. Even though joint probability and its factorization now are more similar, once more the estimate from the simulation match the analytical expression $p(v_i, v_j)$.

Overall, this brief analysis showed us how the bursty behavior that we see for small values of \mathcal{D}^* emerges from the underlying probability distributions, which in turn emerge from the simple marginalization that occurs in Eq. (S2). Similar arguments, albeit impractical, could be carried out for the probability distributions beyond the two-point ones. In a sense, one could argue that the fundamental properties of the model are inherited from the fact that there are some unobserved physical quantities, and these are the quantities that drive the global response of the single variables.

For the specific case of a double Ornstein-Uhlenbeck process we chose, the net effect of the marginalization is the widening of the tails of both the one-point $p(v)$ and the two-point $p(v_i, v_j)$ probability distributions when \mathcal{D}^* is small enough. As we increase \mathcal{D}^* , this effect becomes less and less important until it is completely negligible. In this sense, we can effectively think of \mathcal{D}^* as a control parameter that changes the qualitative behavior of the system. Most importantly, the fact that the tails of the joint probability distribution are wider when \mathcal{D}^* is small reflects dynamically in the emergence of a non trivial coordination between the variables, from which in turn power-law avalanches emerge.

D. THE TIME-DEPENDENT ORNSTEIN-UHLEBECK PROCESS AND THE LYAPUNOV EQUATION

The process studied in the main text is a multivariate Ornstein-Uhlenbeck process [61] of the form

$$d\mathbf{v}(t) = -A\mathbf{v}(t)dt + B(t)d\mathbf{W}(t), \quad (\text{S10})$$

where in our case $B(t)$ is a diagonal matrix whose diagonal elements are given by $\sqrt{\mathcal{D}(t)}$. In the case of decoupled units, which we use to model the extrinsic activity, the matrix A is again diagonal with entries $A_{ij} = \delta_{ij}/\gamma_i$, while if we introduce a connectivity matrix W between the neurons we have $A_{ij} = \frac{\delta_{ij}}{\gamma_i} - W_{ij}$. Note that the latter case is entirely equivalent to the linearized version of a noisy neural network of Wilson-Cowan type [49], with the addition

that in our case a non-trivial, time varying source of noise is present. The formal solution of this stochastic process is given by

$$\mathbf{v}(t) = \exp(-At) \mathbf{v}(0) + \int_0^t \exp[-A(t-t')] B(t') d\mathbf{W}(t').$$

In particular, since in our case the matrix B is on itself a stochastic variable, from now on we will focus on the original variables conditioned on B , which in turn we assume follows its own stationary distribution $p(B)$. We call these conditioned variables $\mathbf{v}(t, B)$. If the eigenvalues of A have all positive real parts, a stationary solution of Eq. S10 exists and it is of the form [62]

$$\mathbf{v}_s(t, B) = \int_{-\infty}^t \exp[-A(t-t')] B d\mathbf{W}(t').$$

Hence, the stationary covariance matrix conditioned on B reads as

$$\begin{aligned} \sigma(B) &= \langle \mathbf{v}_s(t, B), \mathbf{v}_s^T(t, B) \rangle \\ &= \int_{-\infty}^t dt' \exp[-A(t-t')] B B^T \exp[A^T(t-t')] \end{aligned}$$

which solves the algebraic equation

$$A\sigma(B) + \sigma(B)A^T = M,$$

where the matrix M is given by

$$M = \int_{-\infty}^t A \exp[-A(t-t')] B B^T \exp[-A^T(t-t')] dt' + \int_{-\infty}^t \exp[-A(t-t')] B B^T \exp[-A^T(t-t')] A^T dt'.$$

We we can rewrite it as

$$M = \int_{-\infty}^t \frac{d}{dt'} \left\{ \exp[-A(t-t')] B B^T \exp[-A(t-t')] \right\} dt'$$

Carrying out the integral, we find that the lower limit vanishes due to the assumed positivity of the eigenvalues of A and hence only the upper limit remains, giving

$$A\sigma(B) + \sigma(B)A^T = B B^T, \quad (\text{S11})$$

which is a continuous Lyapunov equation [63] for the covariance matrix $\sigma(B)$. Then, we only need to marginalize over B and we obtain the equation for the covariance matrix of our original variables $\mathbf{v}_s(t)$

$$A\sigma + \sigma A^T = Q, \quad (\text{S12})$$

where for the sake of brevity we call σ the covariance matrix of the original variables and Q is a diagonal matrix whose elements are given by

$$Q_{ij} = \delta_{ij} \int_{\mathcal{D}^*} \mathcal{D} p(\mathcal{D}) d\mathcal{D} := \delta_{ij} f(\mathcal{D}^*, \gamma_D, \theta). \quad (\text{S13})$$

Thus, the inverse problem of reconstructing the connectivity matrix from the data reduces to solving numerically Eq. (S12), starting from the correlation matrix of the data and given a set of parameters for the model.

Hence we end up with a model

$$\dot{v}_i(t) = - \sum_j A_{ij} v_j(t) + \sqrt{\mathcal{D}(t)} \xi_i(t) \quad (\text{S14})$$

where A_{ij} depends on the the parameters of the stochastic modulation $(\mathcal{D}^*, \gamma_D, \theta)$. Notice that if we write $\tilde{A}_{ij} = A_{ij}/f(\mathcal{D}^*, \gamma_D, \theta)$ we need to solve the Lyapunov equation $\sigma \tilde{A} + \tilde{A} \sigma = \mathcal{K}$ that only depends on σ , the correlation matrix of the data. If we introduce $\tilde{\mathcal{D}} = \mathcal{D}/f$ and $\tilde{x}_i = x_i/\sqrt{f}$ we can write

$$\dot{\tilde{x}}_i(t) = - \sum_j \tilde{A}_{ij} \tilde{x}_j(t) + \sqrt{\tilde{\mathcal{D}}(t)} \xi_i(t)$$

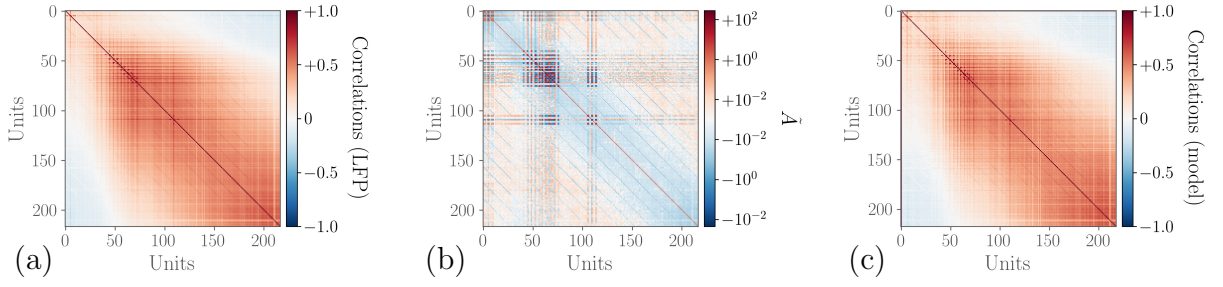


FIG. S4. Comparison between (a) the correlations of the data and (c) the correlations of the interacting model after solving the inverse problem. Panel (b) shows the inferred matrix \hat{A} , which is independent on the parameters of the model.

and clearly

$$\langle \tilde{x}_i \tilde{x}_j \rangle - \langle \tilde{x}_i \rangle \langle \tilde{x}_j \rangle = \frac{\langle x_i x_j \rangle - \langle x_i \rangle \langle x_j \rangle}{f}$$

so the correlation between \tilde{x}_i and \tilde{x}_j is the same of the correlation between x_i and x_j . This means that at different (D^*, θ, γ_D) we simply find a rescaled interaction matrix A_{ij} , but the correlations do not change.

E. SCALING OF THE CORRELATION LENGTH

To study if the correlations of the system under study exhibit critical-like properties we determine the correlation length ξ of the system at various system's sizes. The correlation length is the average distance at which the correlations of the fluctuations around the mean crosses zero [52], and it is known to diverge at criticality in the thermodynamic limit [28].

For finite systems, however, this behavior can be demonstrated by showing that the correlation length grows with system size. Thus, we first compute for each time series their fluctuations around the mean, namely

$$\tilde{v}_i(t) = v_i(t) - \frac{\sum_{i=1}^N v_i(t)}{N} \quad (\text{S15})$$

where $1/N \sum_{i=1}^N v_i(t)$ is the mean activity, i.e. the mean at time t computed over the N channels, and v_i is the activity at channel i . By definition the mean of the fluctuations vanishes, i.e. $\sum_{i=1}^N \tilde{v}_i(t) = 0, \forall t$. As said, different sizes (portions of the array) of the system are selected and, importantly, the mean activity is computed for each system size, considering the channels inside the observation window.

In particular, since the maximum system size (corresponding to N channels) both in our experimental data and in our model is fixed, we investigate how ξ changes with system sizes corresponding to different subsamples from the multi-array probe [64]. In fact, through simulations on control models that display a critical point [65], subsampling has been shown to be practically equivalent to consider systems of different sizes.

In our case the array shape is rectangular of dimensions 55×4 channels, thus we consider the number of rows as the relevant dimension and build subsampled systems of size $L \times 4$, with L that decreases from the maximum of 55 channels up to 5 channels. Next, for each system's subset, we compute the average correlation function of the fluctuations between all pairs of channels separated by a distance r ,

$$\langle C(r) \rangle = \left\langle \frac{\langle (\tilde{v}_i - \bar{v}_i) (\tilde{v}_j - \bar{v}_j) \rangle_t}{\sigma_{\tilde{v}_i} \sigma_{\tilde{v}_j}} \right\rangle_{i,j} \quad (\text{S16})$$

where $\langle \cdot \rangle_t$ stands for the average over time, $\langle \cdot \rangle_{i,j}$ the average over all pairs of channels separated by a distance r and

$$\bar{v}_i = \frac{1}{T} \sum_{t=1}^T \tilde{v}_i(t)$$

$$\sigma_{\tilde{v}_i}^2 = \frac{1}{T} \sum_{t=1}^T (\tilde{v}_i(t) - \bar{v}_i)^2$$

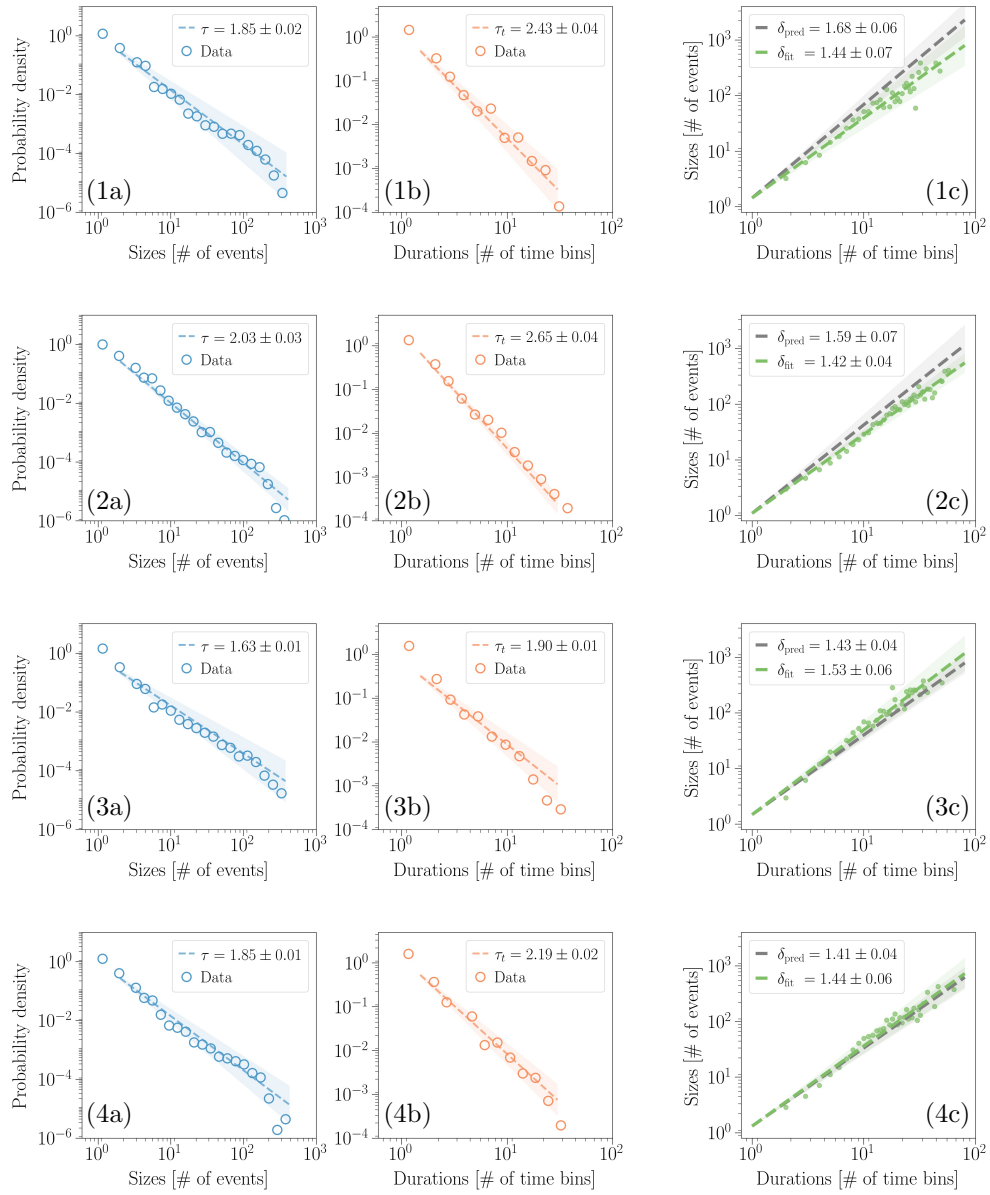


FIG. S5. Avalanche statistics in four different rats. (1a-4a) The distribution of the avalanches' sizes is consistently a power-law, with an exponent that slightly depends on the single rat. (1b-4b) The avalanche durations are once more power-law distributed in all rats with some variability in the exponents, even though the range accessible with the experimental setup only covers two decades. (1c-4c) The crackling-noise relation, however, is consistently satisfied in each rat.

with T is the length of the time series. Then ξ is computed as the zero of the correlation function $C(r = \xi) = 0$. To reduce the noise effects, results were averaged across all possible sub-regions for any given size. Then the ξ are plotted against the relative system size L and the slope of the fit is obtained through a linear regression.

F: AVALANCHES STATISTICS IN LFPS DATA

Here we report the avalanches statistics from the other rats that we analyzed. The avalanches statistics is computed by considering all available the 20 trials of basal activity for each rat, that are 7.22s long. Results are reported in Figure S5. Inter-rat variability is present with respect to avalanche exponents, and is expected as found in previous experiments [23, 66, 67]. Moreover, a theoretical explanation for the difference in avalanche exponents has been also recently proposed as signature of quasi-criticality [50]. However, the fundamental point is that the crackling-noise

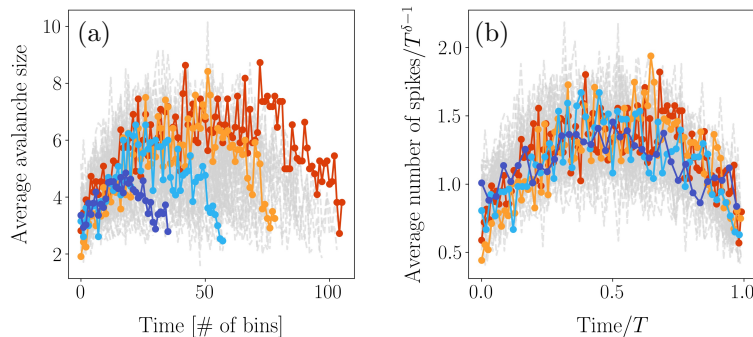


FIG. S6. Collapse of the average profile of avalanches of varying duration in the extrinsic model, for the low \mathcal{D}^* regime. (a) Profile of the avalanches before the rescaling. (b) If we rescale with an exponent $\delta \approx 1.33$, which is remarkably close to the one found in the main text through the crackling-noise relation, we obtain an optimal collapse onto the same scaling function.

relation is always verified compatibly with the experimental errors, a feature that is usually considered a hallmark of criticality [23].

G: ADDITIONAL AVALANCHES STATISTICS IN THE MODEL

Another signature of criticality is the collapse of the average profile of avalanches of widely varying duration onto a single scaling function. For avalanches of duration T we can write down the average number of firing at time t as $s(t, T) = T^{\delta-1}F(t/T)$ where F is a universal scaling function that determines the shape of the average temporal profile. $\langle S(T) \rangle$ and $s(t, T)$ are related by $\langle S(T) \rangle = \int_0^T s(t, T) dt$. Therefore, at the critical point we expected that plots of t/T versus $s(t, T)T^{1-\delta}$ for different T will collapse onto the same universal scaling function [26].

Thus, finding the exponent for which the goodness of the collapse is higher provides another way to estimate δ . For testing the avalanche shape collapse, we used the methodology introduced in [48]. To determine the quality of the collapse, the averaged and rescaled avalanche profiles of different lifetimes $F(t/T) = T^{1-\delta}s(t/T, T)$ are first linearly interpolated at 1000 points along the scaled duration. The variance across the different $F(t/T)$ is calculated at each interpolated point, and the shape collapse error $\epsilon(\delta)$ is then defined as the mean variance divided by the squared span of the avalanche shapes, where the span equals the maximum minus the minimum value of all rescaled avalanche profiles. In the presented analysis, avalanche shapes of $T > 10$ bins with at least 10 samples were used.

The collapse has been tested on the extrinsic model in the case of low \mathcal{D}^* , and the results are plotted in Figure S6. We find that the exponent that minimizes $\epsilon(\gamma)$ turns out to be ≈ 1.33 , close to the estimates of δ found through the linear fit of average size given duration and through the prediction of the crackling-noise relation in the main text. Again, it is also close to the apparently super-universal exponent found in [23] and in [25]. Finally, we found that the average profile collapse on the scaling function has the form of an inverted parabola, as it has been found also in other experiments [25], and analogously in models of inhomogeneous Poisson processes [19].